

MAPPING GENETIC INFLUENCES ON BRAIN FIBER ARCHITECTURE WITH HIGH ANGULAR RESOLUTION DIFFUSION IMAGING (HARDI)

Ming-Chang Chiang¹, Marina Barysheva¹, Agatha D. Lee¹, Sarah Madsen¹, Andrea D. Klunder¹, Arthur W. Toga¹, Katie L. McMahon², Greig I. de Zubicaray², Matthew Meredith², Margaret J. Wright³, Anuj Srivastava⁴, Nikolay Balov⁴, Paul M. Thompson¹

¹Laboratory of Neuro Imaging, Department of Neurology, UCLA School of Medicine, Los Angeles, CA

²Functional MRI Laboratory, Centre for Magnetic Resonance, University of Queensland, Brisbane, Australia

³Queensland Institute of Medical Research, Brisbane, Australia

⁴Department of Statistics, Florida State University, Tallahassee, FL

ABSTRACT

We report the first 3D maps of genetic effects on brain fiber complexity. We analyzed HARDI brain imaging data from 90 young adult twins using an information-theoretic measure, the Jensen-Shannon divergence (JSD), to gauge the regional complexity of the white matter fiber orientation distribution functions (ODF). HARDI data were fluidly registered using Karcher means and ODF square-roots for interpolation; each subject's JSD map was computed from the spatial coherence of the ODFs in each voxel's neighborhood. We evaluated the genetic influences on generalized fiber anisotropy (GFA) and complexity (JSD) using structural equation models (SEM). At each voxel, genetic and environmental components of data variation were estimated, and their goodness of fit tested by permutation. Color-coded maps revealed that the optimal models varied for different brain regions. Fiber complexity was predominantly under genetic control, and was higher in more highly anisotropic regions. These methods show promise for discovering factors affecting fiber connectivity in the brain.

Index Terms— High angular resolution diffusion imaging, DTI registration, Jensen-Shannon divergence, structural equation model, twins

1. INTRODUCTION

High angular resolution diffusion imaging (HARDI) reveals more information on water diffusion and fiber connectivity than conventional diffusion tensor imaging (DTI) because it applies many, usually 30-100, diffusion-encoded gradients to resolve diffusion profiles at higher angular resolution. This advantage, however, becomes a barrier to data mining on HARDI: for a single subject the HARDI dataset is four-dimensional, with one 3D volume of data collected for each gradient direction. This makes intersubject registration and other group analyses of HARDI data very difficult.

In this paper we register the HARDI data of 90 twin subjects by applying tensor-based fluid registration to their corresponding DTI [1]. We also propose a new local measure of fiber complexity based on information theory, the Jensen-Shannon divergence (JSD) [2] to examine the complexity of the local angular structure of diffusion. Our results show that this is powerful for identifying regional diffusion complexity in a large HARDI study.

In neuroscience research, twin studies are informative for understanding the genetic control of brain structure and function. Several aspects of brain morphometry are under strong genetic control, such as cortical thickness [3], and regional gray and white matter (WM) volumes [4]. However, there are no known maps of genetic influences on diffusion profiles or fiber complexity in the brain. Only one study has examined genetic influences on DTI, and found that the proportion of genetic and environmental control varied regionally, for the fractional anisotropy of the corpus callosum [5]. Here we propose a new method for quantitative genetic modeling of HARDI data, combining structural equation models (SEM) and permutation methods to plot the 3D profile of genetic and environmental effects. To our knowledge, these are the first 3D maps of genetic influences on DTI.

2. METHODS

2.1. Subject description and image acquisition

The HARDI data were acquired from 22 pairs of monozygotic (MZ; 20 males/24 females; age = 25.1±1.5 years) and 23 pairs of dizygotic twins (DZ; all were same-sex pairs; 20 males/26 females; age = 23.5±2.2 years) on a 4T Bruker Medspec MRI scanner using an optimized diffusion tensor sequence [6]. Imaging parameters were: 21 axial slices (5 mm thick), FOV = 23 cm, TR/TE 6090/91.7 ms, 0.5 mm gap, with a 128×100 acquisition matrix. Thirty images were acquired: three scans with no diffusion sensitization (i.e., T2-weighted images) and 27 diffusion-weighted images in which the gradient directions were evenly distributed on the hemisphere [6]. The reconstruction matrix was 128×128, yielding a 1.8×1.8 mm² in-plane resolution. The total scan time was 3.05 minutes.

2.2. DTI registration

For each subject, DT images (denoted by D_{ij} , $1 \leq i, j \leq 3$) were computed from the HARDI signals using MedINRIA software (<http://www-sop.inria.fr/asclepios/software/MedINRIA>). One diagonal component image (D_{11}) was manually stripped of nonbrain tissues, yielding a binary brain extraction mask (cerebellum included). The masked image was then registered to the ICBM53 average brain template with a 12-parameter linear transformation using the software FLIRT [7], and resampled to isotropic voxel resolution (dimension: 128×128×93 voxels, resolution: 1.7×1.7×1.7 mm³). The resulting transformation parameters were used to rotationally reorient the tensor at each voxel [8], and then affine align the tensor-valued images based on

This work was funded in part by NIH grant R01 HD050735.

trilinear interpolation of the log-transformed tensors [9]. All affine-registered DT images were then registered to a randomly selected subject's image (a MZ subject), using an inverse-consistent fluid registration algorithm that minimizes the symmetrized Kullback-Leibler divergence (sKL-divergence) of the two tensor-valued images [1].

2.3. HARDI processing and registration

Orientation distribution functions (ODF) for water diffusion were computed voxelwise from the HARDI signals using the Funk-Radon Transform (FRT) [10]. We used Descoteaux's method [11], which first expands the HARDI signals as a spherical harmonic (SH) series, simplifying the FRT to a linear matrix operation on the coefficients. To estimate the SH coefficients, we set the order of the SH series to 4, and added a Laplacian smoothing regularizer to reduce the noise level, and also a Laplacian sharpening regularizer to help detect the peaks of the ODF, as detailed in [11]. The estimated ODF was normalized to unit mass, creating a diffusion probability density function (PDF) parameterized by spherical angle.

Images of the diffusion ODFs were registered to the target subject by applying the corresponding DTI mapping (both affine and fluid mappings) in the previous section. To keep the direction of the diffusion ODFs oriented with the direction of the underlying fibers, ODFs were reoriented using the Preservation of Principal Direction (PPD) method [8], where the principal direction of the ODF was determined based on principal component analysis of the ODF [12]. A generalized fractional anisotropy (GFA) map was constructed from the registered ODF ψ [10]:

$$GFA = \sqrt{n \sum_{i=1}^n (\psi(\mathbf{u}_i) - \langle \psi \rangle)^2} / \sqrt{(n-1) \sum_{i=1}^n \psi(\mathbf{u}_i)^2}. \quad (1)$$

Here \mathbf{u}_i , $1 \leq i \leq n$, are n gradient directions, and $\langle \psi \rangle$ is the mean of the ODF with respect to spherical angle.

Spatial interpolation of HARDI ODFs is a new issue, and is required when the registration mapping falls on non-lattice points. We addressed this by taking the square root of the ODF: the Riemannian manifold for the square root of a PDF is isomorphic to a unit sphere and there are closed form expressions defining the geodesic distance, exponential and inverse exponential mappings [13]. The interpolated square-rooted ODF (sqrt-ODF) ϕ at point (x, y, z) was then constructed by finding the weighted Karcher mean of its 8 diagonal neighbors ϕ_i in 3D at lattice points (x_i, y_i, z_i) , which minimizes the square sum of the geodesic distance d :

$$\phi = \arg \min \sum_{i=1}^8 w_i d(\phi, \phi_i)^2. \quad (2)$$

Here w_i is the trilinear interpolation weight defined as $w_i = (1 - |x - x_i|)(1 - |y - y_i|)(1 - |z - z_i|)$. The weighted Karcher mean ϕ was computed using a gradient descent approach as detailed in [13].

2.4. Measuring regional complexity of diffusion

We defined the regional complexity of diffusion using the generalized Jensen-Shannon divergence (JSD) [2]. JSD measures the dissimilarity of n probability distributions, given by

$$JSD_w(\mathbf{p}_1, \dots, \mathbf{p}_n) = H\left(\sum_{i=1}^n w_i \mathbf{p}_i\right) - \sum_{i=1}^n w_i H(\mathbf{p}_i). \quad (3)$$

Here $\mathbf{p}_i = \{p_{ij}, 1 \leq j \leq k | \sum_{j=1}^k p_{ij} = 1\}$, and $w = \{w_i, 1 \leq i \leq n | \sum_{i=1}^n w_i = 1\}$. $H(\bullet)$ is the Shannon entropy, defined as $H(\mathbf{p}) = -\sum_{j=1}^k p_j \log p_j$. $JSD_w(\mathbf{p}_1, \dots, \mathbf{p}_n) = 0$ if and only if all $\mathbf{p}_1, \dots, \mathbf{p}_n$ are equal. The complexity of diffusion at voxel \mathbf{x} was then defined as the JSD for the ODF at \mathbf{x} and its contiguous 26 ODFs. We adopted an equal weight of $1/n$ for simplicity.

2.5. Statistical analysis of structural models for twins

For analyzing genetic and environmental correlations in twins, the use of structural equation modeling (SEM) is widely accepted [4, 14]. SEM evaluates contributions of additive genetic (A), shared environmental (C) and random environmental (E) components to the covariances of the observed variables (y) for MZ and DZ twins, according to the following model:

$$y_j = aA_j + cC_j + eE_j, \quad (4)$$

where $j = 1$ or 2 for the first or second twin in the same pair. Since A , C , and E are unobservable variables, their weights $\theta = (a, c, e)$ were estimated by comparing the covariance matrix implied by the model (denoted by $\Sigma(\theta)$) and the sample covariance matrix of the observed variables (denoted by \mathbf{S}), using maximum-likelihood fitting:

$$F_{ML,\theta} = \log|\Sigma(\theta)| + \text{trace}(\Sigma^{-1}(\theta)\mathbf{S}) - \log|\mathbf{S}| - p, \quad (5)$$

where p is the number of observed variables, and $p = 2$. Under the null hypothesis that the population covariance matrix of the observed variables equals $\Sigma(\theta)$, and the n -sample data y are multivariate normal, $T_{ML,\theta} = (n-1)F_{ML,\theta}$ follows a chi-squared distribution with $p(p+1)-t$ degrees of freedom, where t is the number of free model parameters. Acceptance of the null hypothesis ($p > 0.05$) indicates a good fit for the model.

Parameter fitting based on the above chi-squared distribution, however, may be biased if the sample data are non-normal. To make SEM free of distributional assumptions, we used permutation methods to determine the goodness of fit [15]. At each voxel, the GFA or JSD of the diffusion ODFs served as the observed variable, with the subject's age regressed out. We computed $T_{ML,\theta}$ using the Broyden-Fletcher-Goldfarb-Shanno (BFGS) method [16] to minimize F_{ML} in (5) in the original sample, as well as in permuted samples in which the twin pairs' MZ or DZ labels were randomly shuffled. The number of permutations was set to 2000. On each permutation relabeling, four null hypotheses with different θ were evaluated, for fitting the E: $\theta = (e)$, CE: $\theta = (c, e)$, AE: $\theta = (a, e)$, and ACE: $\theta = (a, c, e)$ models, and the p -values, p_E, p_{CE}, p_{AE} , and p_{ACE} , were determined separately by comparing $T_{ML,\theta}$ in the true labeling to the permutation distribution. We noticed that, since the permutation distribution of the chi-squared statistic $T_{ML,\theta}$ might be different from its original distribution, rescaling of the sample data using the Bollen-Stine transformation was necessary for each null hypothesis [15]:

$$\mathbf{Z} = \mathbf{Y}\mathbf{S}^{-1/2}\Sigma^{1/2}(\theta). \quad (6)$$

Here \mathbf{Y} is an $n \times 2$ matrix of the observed variables for the n pairs of twins. The square root of a matrix was computed from its Cholesky factorization. The rows of \mathbf{Z} instead of \mathbf{Y} were then permuted.

The four permutation p -values, p_E , p_{CE} , p_{AE} , and p_{ACE} , were compared at each voxel and the voxel was assigned to one of E, CE, AE, and ACE models if the p -value for that model was greater than the other three and also greater than 0.05. We used a color-coded map to visualize the optimal model fitted at each voxel, with E coded as blue, CE as green, AE as red, and ACE as yellow. For better visualization, we defined “model clusters”, defined as sets of connected (26-neighborhood) voxels of the same model, for each of the four models, and only displayed clusters that contained more than 10,000 voxels.

3. RESULTS

Fig. 1 displays the spatial distribution of the average JSD (averaged across all 90 subjects). The value of the average JSD increases with GFA, which indicates that JSD is sensitive to the complexity of ODFs in major white matter fibers with high diffusion anisotropy, especially in regions where the anisotropy values vary over a small spatial neighborhood. In regions of low anisotropy, the ODF shape is closer to a unit sphere so those ODFs are more alike. This property of JSD is useful because in DTI/HARDI studies, researchers are typically more interested in the diffusion properties of highly anisotropic brain regions, where fiber structures are highly resolved.

Fig. 2 and 3 show the covariance structure fitting for maps of GFA and JSD in the 90 twins. When the AE model fits best, the variation in GFA or JSD values is more attributable to genetic influences, i.e., the covariance structures of GFA or JSD at that voxel are best accounted for by additive genetic (added effect of genes) and random environmental effects (random experimental error is also lumped into the E term). When the CE model fits best, the variation in the observed measures is more due to environmental influences shared by twins reared in the same family [14]. The full ACE model, in which all terms fit at once, could not be fitted for either GFA or JSD. For both GFA and JSD measures, more voxels had AE as the best-fitting model than CE or any other model, indicating that diffusion properties are more genetically influenced than environmentally influenced, in most brain regions.

Our results also suggested that there may be some hemispheric asymmetry in model fitting, e.g. in the cingulum. Variation in GFA or JSD in the left cingulum (**Fig. 2a, circled**) is more explained by the shared environment (CE), while the right cingulum more by the additive genetic effect (AE). In our previous twin study, we also found asymmetry in the degree of genetic control for the thickness of the language-related cortex [3]. Taken together, this suggests that genetic influences on different brain regions may be asymmetric; this hypothesis will be tested formally and verified on a larger sample, by entering hemisphere as a covariate of interest in a more complex structural equation model.

4. CONCLUSION

This study unites four key mathematical concepts to provide a processing pipeline for population studies of HARDI; we used the pipeline to create the first maps of genetic influences on fiber architecture in the living brain. HARDI is a special type of multi-valued medical image, with a spherical function of diffusion-sensitive signals at each voxel. To analyze this high-dimensional

data, we used fluid image registration to align data across subjects, driven by a tensor-valued information theory metric (sKL-divergence). This ensured good anatomical fiber correspondence across subjects before comparing and integrating data across a population. To preserve angular detail, we used a spectral implementation of the Funk-Radon transform, ODF sharpening, ODF square-root transformation, and Karcher means, to convect the signals through the fluid mapping and resample them in appropriate Riemannian manifolds. Third, we computed maps involving new measures of fiber integrity (GFA) and fiber spatial coherence (JSD), that exploit the full angular detail obtainable with HARDI. Fourth, we estimated quantitative genetic models by fitting a standard ACE design at each voxel, but developing a new permutation method based on the Bollen-Stine transformation to avoid making the strong assumption that the model residuals were chi-squared distributed random fields.

Our neuroscientific results suggested that: (1) fiber measures are highly genetically controlled, especially in regions of high diffusion anisotropy, (2) there are also environmental effects on fiber morphology, in different brain regions, with possible hemispheric asymmetries; and (3) the genetic fit is strong enough that future studies may be able to detect individual genes contributing to fiber architecture, using these measures and algorithms to guide the search.

REFERENCES

- Chiang, M.-C., et al., *Fluid registration of diffusion tensor images using information theory*. IEEE Transactions on Medical Imaging, 2008 (In Press).
- Lin, J., *Divergence measures based on the Shannon entropy*. IEEE Transactions on Information Theory, 1991. **37**(1): p. 145-151.
- Thompson, P.M., et al., *Genetic influences on brain structure*. Nat Neurosci, 2001. **4**(12): p. 1253-8.
- Schmitt, J.E., et al., *A multivariate analysis of neuroanatomic relationships in a genetically informative pediatric sample*. Neuroimage, 2007. **35**(1): p. 70-82.
- Pfefferbaum, A., E.V. Sullivan, and D. Carmelli, *Genetic regulation of regional microstructure of the corpus callosum in late life*. Neuroreport, 2001. **12**(8): p. 1677-81.
- Jones, D.K., M.A. Horsfield, and A. Simmons, *Optimal strategies for measuring diffusion in anisotropic systems by magnetic resonance imaging*. Magn Reson Med, 1999. **42**(3): p. 515-25.
- Jenkinson, M. and S. Smith, *A global optimisation method for robust affine registration of brain images*. Med Image Anal, 2001. **5**(2): p. 143-56.
- Alexander, D.C., et al., *Spatial transformations of diffusion tensor magnetic resonance*. IEEE Transactions on Medical Imaging, 2001. **20**: p. 1131-1139.
- Arsigny, V., et al., *Fast and simple calculus on tensors in the log-Euclidean framework*, in *Int Conf Med Image Comput Comput Assist Interv (MICCAI)*. 2005. p. 115-22.
- Tuch, D.S., *Q-ball imaging*. Magn Reson Med, 2004. **52**(6): p. 1358-72.
- Descoteaux, M., et al., *A linear and regularized ODF estimation algorithm to recover multiple fibers in Q-Ball imaging*. Research Report No. 5768, 2005, INRIA Sophia Antipolis.

12. Chiang, M.-C., et al., *Information-theoretic analysis of brain white matter fiber orientation distribution functions*, in *Information Processing in Medical Imaging*. 2007: Kerkrade, The Netherlands. p. 172-182.
13. Srivastava, A., I. Jermyn, and S.H. Joshi. *Riemannian Analysis of Probability Density Functions with applications in Vision*. In *IEEE Computer Society Conference on Computer Vision and Pattern Recognition (CVPR)*. 2007. Minneapolis, Minnesota, USA.
14. Neale, M.C., L.R. Cardon, and North Atlantic Treaty Organization Scientific Affairs Division, *Methodology for genetic studies of twins and families*. 1992, Dordrecht ; Boston: Kluwer Academic Publishers. xxv, 496 p.
15. Bollen, K.A. and R.A. Stine, *Bootstrapping goodness-of-fit measures in structural equation models*. Sociological Methods Research, 1992. **21**(2): p. 205-229.
16. Press, W.H., et al., *Numerical recipes in C++*. 2nd ed. 2002, Cambridge, [England]; New York: Cambridge University Press. viii, 318 p.

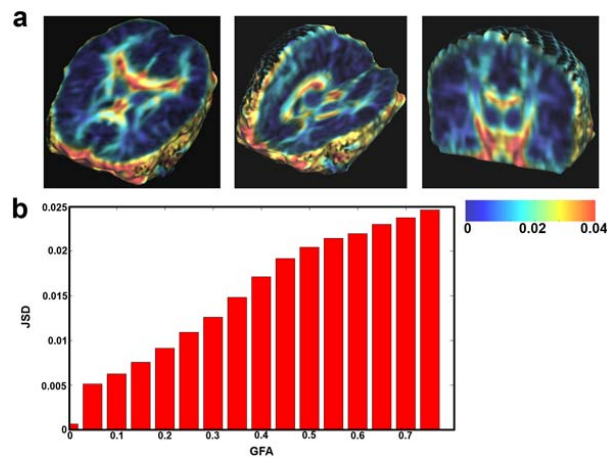


Fig. 1. (a) The color-coded map shows that the JSD, a measure of fiber complexity, is greater in regions of high diffusion anisotropy (e.g., the corpus callosum), especially at interfaces between high and low anisotropy. This trend becomes clear when plotting JSD against the GFA in (b).

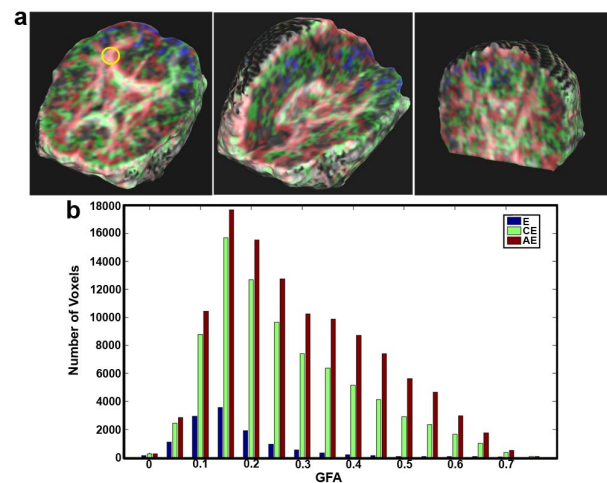


Fig. 2. (a) The color-coded map shows which model fits best for the covariance matrices of GFA, a measure of fiber integrity, at each voxel. Voxels with covariance matrices of GFA in MZ and DZ twins where the E model fitted best are coded as blue, CE is coded as green, and AE is coded as red. Major fiber structures with high GFA values, such as the corpus callosum, cingulum, and internal capsules, are optimally fitted using the AE and the CE models. There is a visible asymmetry in model fitting in the cingulum fibers, where the right cingulum is better fitted by the AE model (yellow circle), while the left cingulum is better fitted by the CE model. (b) A histogram shows the number of voxels where the best-fitting model is E, CE, or AE (only those clusters composed of more than 10,000 voxels were included). Plotting this against the GFA shows that the AE and the CE models explain the covariance structures of GFA in highly anisotropic regions, while the E model fits best in low-anisotropy regions. As genetics (rather than environment) is the predominant influence on these fiber measures, specific candidate genes affecting fiber integrity and connectivity may be discoverable in larger samples.

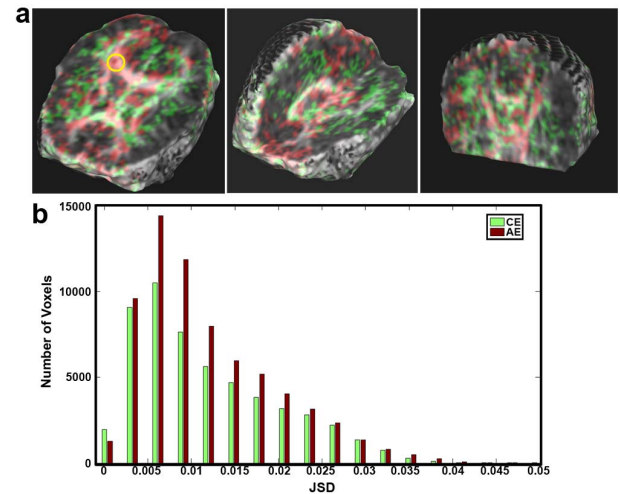


Fig. 3. (a) The color-coded map shows which genetic models best explain variations in fiber complexity (JSD), across 90 individuals. Color coding is the same as in Fig. 2. As with GFA (Fig. 2), there is a visually apparent asymmetry for the cingulum fibers, showing that voxels assigned to the AE model are more prevalent in the right cingulum (circled in yellow), but voxels where the CE model is optimal are found more in the left cingulum. (b) The histogram shows the distribution of the voxel numbers for different models, considering only clusters of size greater than 10,000 voxels. For each JSD value, voxels assigned to the AE model (red) outnumber those assigned to the CE model, and there is no large enough cluster (> 10,000 voxels) for the E model.